Decays of τ leptons to final states containing K_S^0 mesons

T. E. Coan, J. Dominick, V. Fadeyev, I. Korolkov, M. Lambrecht, S. Sanghera, V. Shelkov, R. Stroynowski, I. Volobouev, and G. Wei
Southern Methodist University, Dallas, Texas 75275

M. Artuso, A. Efimov, M. Gao, M. Goldberg, D. He, N. Horwitz, S. Kopp, G. C. Moneti, R. Mountain, Y. Mukhin, S. Playfer, T. Skwarnicki, S. Stone, and X. Xing
Syracuse University, Syracuse, New York 13244

J. Bartelt, S. E. Csorna, V. Jain, and S. Marka
Vanderbilt University, Nashville, Tennessee 37235

A. Freyberger, D. Gibaut, K. Kinoshita, P. Pomianowski, and S. Schrenk
Virginia Polytechnic Institute and State University, Blacksburg, Virginia 24061

D. Cinabro
Wayne State University, Detroit, Michigan 48202

B. Barish, M. Chadha, S. Chan, G. Eigen, J. S. Miller, C. O'Grady, M. Schmidtler, J. Urheim, A. J. Weinstein, and F. Würthwein
California Institute of Technology, Pasadena, California 91125

D. M. Asner, M. Athanas, D. W. Bliss, W. S. Brower, G. Masek, and H. P. Paar
University of California, San Diego, La Jolla, California 92093

J. Gronberg, C. M. Korte, R. Kutschke, S. Menary, R. J. Morrison, S. Nakanishi, H. N. Nelson, T. K. Nelson, C. Qiao, J. D. Richman, D. Roberts, A. Ryd, H. Tajima, and M. S. Witherell
University of California, Santa Barbara, California 93106

R. Balest, K. Cho, W. T. Ford, M. Lohner, H. Park, P. Rankin, J. Roy, and J. G. Smith
University of Colorado, Boulder, Colorado 80309-0390

J. P. Alexander, C. Bebek, B. E. Berger, K. Berkelman, K. Bloom, D. G. Cassel, H. A. Cho, D. M. Coffman, D. S. Crowcroft, M. Dickson, P. S. Drell, D. J. Dumas, R. Ehrlich, R. Elia, P. Gaidarev, R. S. Galik, B. Gittelman, S. W. Gray, D. L. Hartill, B. K. Heltsley, C. D. Jones, S. L. Jones, J. Kandaswamy, N. Katayama, P. C. Kim, D. L. Kreinick, T. Lee, Y. Liu, G. S. Ludwig, J. Masui, J. Mevissen, N. B. Mistry, C. R. Ng, E. Nordberg, J. R. Patterson, D. Peterson, D. Riley, A. Soffer, and C. Ward
Cornell University, Ithaca, New York 14853

P. Avery, C. Prescott, S. Yang, and J. Yelton
University of Florida, Gainesville, Florida 32611

G. Brandenburg, R. A. Briere, T. Liu, M. Saulnier, R. Wilson, and H. Yamamoto
Harvard University, Cambridge, Massachusetts 02138

T. E. Browder, F. Li, and J. L. Rodriguez
University of Hawaii at Manoa, Honolulu, Hawaii 96822

T. Bergfeld, B. I. Eisenstein, J. Ernst, G. E. Gladding, G. D. Gollin, M. Palmer, M. Selen, and J. J. Thaler
University of Illinois, Champaign-Urbana, Illinois 61801

K. W. Edwards, K. W. McLean, and M. Ogg
Carleton University, Ottawa, Ontario K1S 5B6 and the Institute of Particle Physics, Canada

A. Bellerive, D. I. Britton, R. Janicek, D. B. MacFarlane, P. M. Patel, and B. Spaan
McGill University, Montréal, Québec H3A 2T8 and the Institute of Particle Physics, Canada

0556-2821/96/53(11)/6037(17)/$10.00

A. J. Sadoff
Ithaca College, Ithaca, New York 14850

R. Ammar, P. Baringer, A. Bean, D. Besson, D. Coppage, N. Copty, R. Davis, N. Hancock, S. Kotov, I. Kravchenko, and N. Kwak
University of Kansas, Lawrence, Kansas 66045

Y. Kubota, M. Lattery, J. K. Nelson, S. Patton, R. Poling, T. Riehle, and V. Savinov
University of Minnesota, Minneapolis, Minnesota 55455

M. S. Alam, I. J. Kim, Z. Ling, A. H. Mahmood, J. J. O'Neill, H. Severini, C. R. Sun, S. Timm, and F. Wappler
State University of New York at Albany, Albany, New York 12222

J. E. Duboscq, R. Fulton, D. Fujino, K. K. Gan, K. Honscheid, H. Kagan, R. Kass, J. Lee, M. Sung, A. Undrus,* C. White, R. Wanke, A. Wolf, and M. M. Zoeller
Ohio State University, Columbus, Ohio 43210

X. Fu, B. Nemati, S. J. Richichi, W. R. Ross, P. Skubic, and M. Wood
University of Oklahoma, Norman, Oklahoma 73019

M. Bishai, J. Fast, E. Gerndt, J. W. Hinson, T. Miao, D. H. Miller, M. Modesitt, E. I. Shibata, I. P. J. Shipsey, and P. N. Wang
Purdue University, West Lafayette, Indiana 47907

L. Gibbons, S. D. Johnson, Y. Kwon, S. Roberts, and E. H. Thorndike
University of Rochester, Rochester, New York 14627

C. P. Jessop, K. Lingel, H. Marsiske, M. L. Perl, S. F. Schaffner, and R. Wang
Stanford Linear Accelerator Center, Stanford University, Stanford, California 94309

(CLEO Collaboration)

(Received 10 January 1996)

Using data collected with the CLEO II detector at the Cornell Electron Storage Ring, we have studied the decays of τ leptons produced through e^+e^- annihilation into final states containing K^0_S mesons, observed through their decays to $\pi^+\pi^-$. We present branching fractions for decays to five final states: $\tau^-\to K^0h^-\nu_\tau$, $\tau^-\to K^0h^-\pi^0\nu_\tau$, $\tau^-\to K^0K^-\nu_\tau$, $\tau^-\to K^0K^-\pi^0\nu_\tau$, and $\tau^-\to K^0_SK^0_Sh^-\nu_\tau$, where K^0h^- denotes the sum of the processes involving $K^0\pi^-$ and K^0K^- particle combinations. Substructure and mass spectra in these final states are also addressed. [S0556-2821(96)04311-1]

PACS number(s): 13.35.Dx, 14.40.Ev, 14.60.Fg

I. INTRODUCTION

Although τ decays to final states with kaons were first observed more than ten years ago, only quite recently have experiments acquired sufficiently large data samples to measure the branching fractions with good precision or to attempt detailed studies of the decay dynamics. There are many interesting issues: tests of Cabibbo suppression, $SU(3)_f$ symmetry breaking [1], and better understanding of the spectral functions [2] and substructure. More precise measurements of kaon modes will allow improved corrections to modes which have been measured without distinguishing between pions and kaons such as $\tau^-\to h^-\nu_\tau$, $\tau^-\to h^-\pi^0\nu_\tau$, or $\tau^-\to h^-h^+h^-\nu_\tau$, where h signifies a charged pion or kaon [3]. The total branching fraction for modes involving kaons, which amounts to a few percent, must be measured well if exclusive decays are to be tabulated accurately [4].

In this article, we report on studies of τ decays to final states containing neutral kaons using data accumulated with the CLEO II detector operating at the Cornell Electron Storage Ring (CESR). We begin by reviewing the phenomenology of the decays under investigation and stating the objectives of our studies. In Sec. II we describe the event selection. A discussion of models used in determining the experimental acceptance follows in Sec. III. In Secs. IV and V we present the measurements of the branching fractions and explain our estimates of the various systematic errors. We show the reconstructed invariant mass spectra in Sec. VI, comparing with the predictions of various models. The article concludes with a discussion of the results and a summary in Secs. VII and VIII.

*Permanent address: BINP, RU-630090 Novosibirsk, Russia.

A. The decay $\tau \to \bar{K}\pi\nu_\tau$

By analogy with τ decays in the nonstrange sector, the $\tau \to KX$ mode with the largest branching fraction is expected to be $\tau \to K\pi\nu_\tau$. The $K\pi$ final state is the Cabibbo-suppressed analogue of the $\pi\pi$ system in $\tau \to \pi\pi\nu_\tau$ decay, and both are expected to be produced predominantly by the vector hadronic currect ($J^P = 1^-$). If one ignores vector current production of strange ($S=1$) systems with three or more mesons, the decay width in terms of the mass squared of the final hadronic state (q^2), the Cabibbo-Kobayashi-Mashawa (CKM) matrix element V_{us}, and the τ mass M_τ, simplifies to [2]

$$\Gamma(\tau^- \to \nu_\tau (\bar{K}\pi)^-_{J^P=1^-}) = \frac{G_F^2}{(2\pi)^2 (2M_\tau)^3} |V_{us}|^2 \times \int_0^{M_\tau^2} dq^2 (M_\tau^2 - q^2)^2 (M_\tau^2 + 2q^2) \times v_1^S(q^2), \quad (1)$$

where $v_1^S(q^2)$ is the vector spectral function with nonzero strangeness. Similar to $\rho(770)$ dominance in the $\pi\pi$ system, the $J^P = 1^-$ $K\pi$ state is expected to be dominated by the $K^*(892)$ resonance, and the spectral function can be approximated, assuming that the K^* width is sufficiently narrow, as

$$v_1^S(q^2) = 2\pi \frac{f_{K^*}^2}{q^2} \delta(q^2 - M_{K^*}^2), \quad (2)$$

where f_{K^*} is the K^* decay constant. The corresponding nonstrange spectral function $v_1(q^2)$ can be obtained by replacing f_{K^*} with f_ρ, M_{K^*} with M_ρ, and V_{us} with V_{ud}.

In the case of exact SU(3)$_f$ symmetry, $f_{K^*} = f_\rho$. Although this symmetry is broken, from one of the Das-Mathur-Okubo (DMO) sum rules [1] one can derive a relationship between the decay constants, assuming that the spectral functions are dominated by a single narrow resonance:

$$\int dq^2 [v_1(q^2) - v_1^S(q^2)] = 0 \Rightarrow \frac{f_{K^*}^2}{M_{K^*}^2} = \frac{f_\rho^2}{M_\rho^2}. \quad (3)$$

This leads to the relation

$$\frac{\mathcal{B}(\tau^- \to K^{*-}\nu_\tau)}{\mathcal{B}(\tau^- \to \rho^-\nu_\tau)} = 0.93 \left| \frac{V_{us}}{V_{ud}} \right|^2. \quad (4)$$

Taking $\mathcal{B}(\tau^- \to \rho^-\nu_\tau)$ to be $(25.0 \pm 0.4)\%$ [5], $|V_{ud}|$ to be 0.975, and $|V_{us}|$ to be 0.222, Eq. (4) then predicts $\mathcal{B}(\tau^- \to K^{*-}\nu_\tau) = (1.20 \pm 0.02)\%$.

This calculation assumes that the $\bar{K}\pi$ and $\pi\pi$ final states are saturated by the lowest-lying resonances, and neglects contributions from radially excited vector mesons. In the case of $\pi\pi$, contributions from radial excitations of the ρ such as the $\rho(1450)$ resonance (the ρ') are expected [6,7], and have possibly been observed [8,9]. Likewise, it is expected that a $K^{*\prime}$ [for example, the $K^*(1410)$], will also populate the $K\pi$ final state. If, as argued by Finkemeier and Mirkes [10], the relative admixtures of ρ' and $K^{*\prime}$ are comparable, the predictions from the sum rules remain largely unchanged.

In the calculation, τ decays through the vector hadronic current to final states containing more than two mesons have been ignored in Eq. (1). It has been recognized [11,12] that the hadronic system in $\tau \to 4\pi\nu_\tau$ decay is an essential component of the nonstrange vector spectral function. The first Weinberg sum rule [13], $\int dq^2 (v_1(q^2) - a_1(q^2)) = f_\pi^2$, where $a_1(q^2)$ represents the $S=0$ axial-vector spectral function, fails when applied to τ data without the inclusion of the 4π spectrum in v_1 [11]. Similarly, the $S=1$ vector current can contribute to $K\pi\pi$ and $K\pi\pi\pi$ final states, however experimental data and theoretical predictions are limited for these modes.

B. The decay $\tau \to \bar{K}\pi\pi\nu_\tau$

Similar to the $\bar{K}\pi - \pi\pi$ case, $\tau \to \bar{K}\pi\pi\nu_\tau$ is the strange analogue of $\tau \to 3\pi\nu$, and is believed to occur predominantly through the axial-vector hadronic current ($J^P = 1^+$). However, the situation is more complicated in the kaon case since there are two allowed axial-vector states with similar masses: namely the $^3P_1$ and $^1P_1$ states, denoted as K_{1A} and K_{1B}, respectively. These states correspond to the $a_1(1260)$ and $b_1(1235)$ for the nonstrange $\bar{u}d$ final state. In the case of $\bar{u}d$, the decay $\tau^- \to b_1^-\nu_\tau$ is highly suppressed due to G-parity conservation and can occur only through isospin symmetry violation, assuming second-class currents do not exist. However, in the corresponding $\bar{u}s$ case, the broken SU(3)$_f$ symmetry allows K_{1B} production in τ decay along with K_{1A}; their relative amounts is a measure of SU(3)$_f$ symmetry breaking [14].

Experimentally, we do not observe either K_{1A} or K_{1B}. Instead, the observed resonances, denoted by $K_1(1270)$ and $K_1(1400)$, are believed to be mixtures of K_{1A} and K_{1B} [5,14]. Hence, determination of the branching ratios $\mathcal{B}(\tau^- \to K_1^-(1270)\nu_\tau)$ and $\mathcal{B}(\tau^- \to K_1^-(1400)\nu_\tau)$ will allow us to probe both the SU(3)$_f$ symmetry breaking and the K_{1A}-K_{1B} mixing. Furthermore, the $K_1(1270)$ decays to many modes, primarily $K\rho$, while the $K_1(1400)$ decays almost exclusively to $K^*\pi$. Thus, study of the $K\pi\pi$ Dalitz plot will also help untangle the dynamics.

Also in contrast with the 3π case, the absence of an analogue for G parity permits $K\pi\pi$ production via the vector hadronic current, for example, through the $K^*(1410)$, for which the dominant decay mode is $K^*\pi$. In the model of Finkemeier and Mirkes [10], the vector current contribution to $K\pi\pi$ is predicted to be about 10% of the total.

C. The decays $\tau \to K\bar{K}(\pi)\nu_\tau$

The phenomenology of τ decays to two kaons parallels that for decays to one kaon. Although not Cabibbo disfavored, these decays are suppressed because of the limited phase space for producing two kaons. The mode $\tau^- \to K^0 K^-\nu_\tau$ is expected to be dominated by the vector current. Since the final state has zero net strangeness, in principle the spectral function and decay rate could be extracted by applying the conserved vector current (CVC) theorem to data on $e^+e^- \to K\bar{K}$ at low (below M_τ) energies. This is not

feasible since the $K\overline{K}$ state in e^+e^- is predominantly isoscalar (due to the ϕ meson). Instead, $SU(3)_f$ symmetry is used to relate KK to $\pi\pi$; Eidelman and Ivanchenko [15] apply this approach to existing data for $e^+e^-\to\pi^+\pi^-$ to obtain a prediction for $\tau\to KK\nu_\tau$. Taking into account SU(3)-breaking effects such as the $\pi-K$ mass difference, they predict a branching ratio for $\tau\to KK\nu_\tau$ of $(0.12\pm0.03)\%$. In a similar calculation, Narison and Pich [16] obtain a value of $(0.16\pm0.02)\%$.

As with the $K\pi\pi$ final state, the three-meson $KK\pi$ case is considerably more complicated than the two-meson case or the 3π case. Furthermore, theoretical constraints are lacking, and predictions vary considerably depending on input assumptions. Production of the $KK\pi$ system in τ decay can occur through either the vector or axial-vector nonstrange weak hadronic current [17–19]. Gilman and Rhie [17] proposed that this decay might arise through production via the vector current of the ρ', which could decay to $KK\pi$ via K^*K. In a chiral Lagrangian-based model, Gomez-Cadenas, Gonzalez-Garcia, and Pich [18] examine the axial-vector and (anomalous) vector contributions to $\tau^-\to K^-K^+\pi^-\nu_\tau$ with $\rho\pi$ substructure. They conclude that the vector contribution should dominate by a factor of 10. Decker *et al.* [19], in a similarly constructed model, include both K^*K and $\rho\pi$ intermediate states, and find to the contrary that the axial-vector contribution [nominally via the $a_1(1260)$] should dominate. Further refinement of this model by Finkemeier and Mirkes [10] supports this conclusion.

For $\tau^-\to K^0K^0\pi^-\nu_\tau$, an additional issue of relevance to experimental work concerns the coherent evolution of the K^0K^0 system in this decay. The ratio $R\equiv\Gamma(\tau^-\to K_S^0K_S^0\pi^-\nu_\tau)/\Gamma(\tau^-\to K_S^0K_L^0\pi^-\nu_\tau)$ depends on the decay dynamics. If the decay proceeds through an intermediate $\rho^0\pi^-$ (or $\phi\pi^-$) state, for example, then the $K_S^0K_S^0\pi^-$ final state is forbidden by Bose statistics. In the model of Ref. [10], $R\sim0.5$ but depends on the resonance parameters used to describe the decay.

While the dynamics governing $KK\pi$ decays merit study, additional interest in these decays lies in their utility for constraining the mass of the τ neutrino. Because these decays are greatly phase-space suppressed, the $KK\pi$ mass spectrum may be sensitive to a nonzero τ neutrino mass, as events are likely to populate the region near the kinematic end point $M_\tau-M_{\nu_\tau}$. From four $\tau^-\to K^-K^+\pi^-\nu_\tau$ events, DELCO derived the most stringent limit on M_{ν_τ} at that time [20]. However, existing data are insufficient to determine whether $KK\pi$ is more or less sensitive than the also-rare five-pion final states ($\mathcal{B}\sim0.1\%$) which have since provided the best limits (31, 32.6, and 24 MeV) on M_{ν_τ} [21–23].

D. Goals of this study

CLEO II has previously published branching fraction measurements for the decays $\tau^-\to K^-\nu_\tau$, $\tau^-\to K^-\pi^0\nu_\tau$, and $\tau^-\to K^-\pi^0\pi^0\nu_\tau$ [24]. Branching fractions for the decays $\tau^-\to K^{*0}\pi^-\nu_\tau$ and $\tau^-\to K^{*0}K^-\nu_\tau$ obtained with the CLEO 1.5 detector, using the $K^{*0}\to K^+\pi^-$ channel, have also been reported [25]. Here, we present results for the final states [26] $K^0h^-\nu_\tau$, $K^0h^-\pi^0\nu_\tau$, $K^0K^-\nu_\tau$, $K^0K^-\pi^0\nu_\tau$, and $K_S^0K_S^0h^-\nu_\tau$, where neutral kaons are observed through the decay $K_S^0\to\pi^+\pi^-$. The focus of this study is on the determination of branching fractions.

With regard to issues of hadronic structure, we present the observed invariant mass spectra and point out qualitative features for comparison with theoretical models and results from other experiments. Quantitative analyses of the hadronic systems will be reported in a future paper [9].

II. DATA ACCUMULATION AND ANALYSIS

A. Detector and data set

The data included in these analyses were accumulated between November 1990 and September 1993 with the CLEO II detector operating at the CESR e^+e^- collider. Roughly 2/3 of the data were collected on the $\Upsilon(4S)$ resonance at a center-of-mass energy $\sqrt{s}=2E_{\rm beam}\sim10.58$ GeV, with the remainder collected at $\sqrt{s}\sim10.52$ GeV. The integrated luminosity of this sample, 2.96 fb^{-1}, corresponds to 2.71×10^6 produced τ-pair events. For the statistics-limited $K_S^0K_S^0h^-$ channel, we also include 0.69 fb^{-1} of data collected through February 1994 and between July and October 1990, for a total of 3.33×10^6 τ pairs.

The CLEO II detector has been described in detail elsewhere [27]. The components of the detector which are most critical to this study are the three concentric cylindrical drift chambers occupying the space 4 cm to 95 cm radially from the beam axis, comprising a 67-layer charged-particle tracking system which is immersed in a 1.5 Tesla solenoidal magnetic field. This system provides efficient and precise reconstruction of $K_S^0\to\pi^+\pi^-$ decays, since at CESR energies nearly all K_S^0's decay within the first few layers, thus allowing the daughter pions to be tracked. The momentum p, in GeV, of charged particles is measured with a resolution of $\sigma_p/p(\%)\approx[(0.15p)^2+(0.5)^2]^{1/2}$. This corresponds to a typical resolution of ~5 MeV on the invariant mass of the $\pi^+\pi^-$ pair produced in K_S^0 decay. In addition, ionization loss (dE/dx) is measured in the 51-layer main drift chamber with a resolution of 6–7%, permitting some discrimination between charged kaons and pions, as described in detail below.

Also important for the measurements reported here is an electromagnetic calorimeter consisting of 7800 thallium-doped CsI crystals. These crystals, each of dimension ~5 cm$\times5$ cm$\times30$ cm, surround the tracking volume, covering 98% of the full solid angle. Forming the barrel region of the calorimeter, 6144 tapered crystals are arrayed just inside of the magnet coil at a radius of ~1 m in a projective cylindrical geometry, covering 82% of the solid angle. The remaining crystals are rectangular, and are oriented axially in two end caps, overlapping in solid angle with the ends of the barrel. The barrel region of the calorimeter achieves energy and angular resolutions for electromagnetically showering particles of $\sigma_E/E(\%)=0.35/E^{0.75}+1.9-0.1E$ and $\sigma_\phi(\text{mrad})=2.8/\sqrt{E}+2.5$ (E in GeV), respectively. The resulting photon energy and direction information provided by this system is used to reconstruct $\pi^0\to\gamma\gamma$ decays which may accompany the charged tracks, and to veto potential background processes such as $e^+e^-\to q\overline{q}$, in which the photon multiplicity is typically higher than that in τ-pair events.

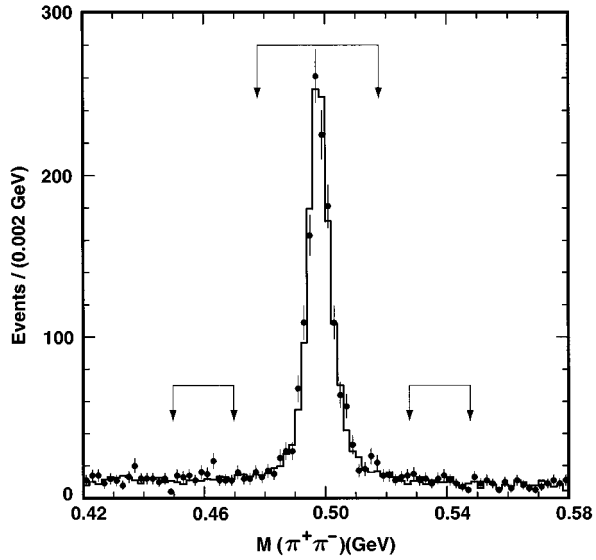

FIG. 1. The invariant mass $M(\pi^+\pi^-)$ for $K_S^0 \to \pi^+\pi^-$ candidates in the $\tau^- \to K_S^0 h^- \nu_\tau$ sample from data (points) and τ Monte Carlo events (histogram). The signal and sideband regions used for event counting are indicated.

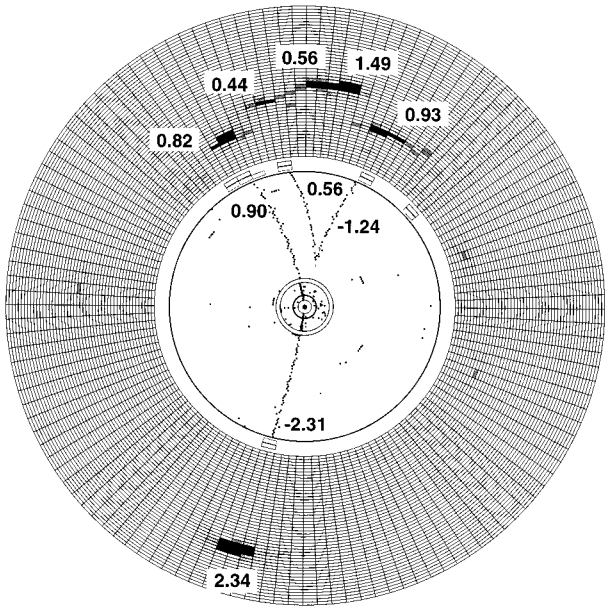

FIG. 2. Axial view of an event containing a $K_S^0 \to \pi^+\pi^-$ decay. This event is a candidate for $e^+e^- \to \tau^+\tau^-$ with a $\tau^+ \to K_S^0 h^+ \pi^0 \overline{\nu_\tau}$ decay recoiling against $\tau^- \to e^- \overline{\nu_e} \nu_\tau$ decay. The locations of struck tracking chamber wires are indicated by dots. The tracks intersecting at the detached vertex form the K_S^0 candidate. The calorimeter is shown in an ''exploded'' view in which increasing radius is actually increasing z. Two nearly overlapping showers at the top of the figure reconstruct to form a π^0 candidate of energy $\sim$2 GeV. The numbers denote charged-particle momenta and shower energies in GeV.

Although not essential to this analysis, the lepton identification capabilities of CLEO II permit classification of decays of the τ lepton recoiling against a final state of interest. Electron identification is based on energy deposition in the calorimeter and dE/dx measurements in the main drift chamber. Muons are identified by their penetration to proportional tubes embedded in magnetic flux return iron, at depths corresponding to three, five, and seven nuclear interaction lengths.

B. Selection of events containing one K_S^0

The primary event selection for all measurements is similar. For brevity, we describe the selection for $\tau^- \to K_S^0 h^- \nu_\tau$ and $\tau^- \to K_S^0 h^- \pi^0 \nu_\tau$ and point to any major difference(s) in the other analyses. In general, we note that in the $K_S^0 h^-$ analysis for which the statistics are largest, more stringent cuts are applied for better control over systematic errors. For other modes, selection criteria are less stringent for higher acceptance.

A sample of $\tau^- \to K_S^0 h^- \nu_\tau$ events is selected by requiring four charged tracks, each with momentum transverse to the beam axis $p_T > 0.05 E_{\rm beam}$ and $|\cos\theta| < 0.8$, where θ is the polar angle of the track relative to the e^+e^- beam axis (z). We define a 1–3 topology by requiring one track to be isolated, making an angle of at least 90° with each of the other three tracks. The isolated track must have $|\cos\theta| < 0.71$ and momentum $p > 0.1 E_{\rm beam}$, to help ensure efficient triggering and reduce potential backgrounds from two-photon processes and beam-gas interactions. To reduce backgrounds from $e^+e^- \to q\overline{q}$ reactions (denoted as $q\overline{q}$ events) and two-photon processes, we require that the net missing momentum of the event be greater than $0.06 E_{\rm beam}$ in the transverse (x-y) plane, and not point within 32° of the beam axis ($|\cos\theta| < 0.85$). We also require the total visible energy in the event to be between $0.7 E_{\rm beam}$ and $1.6 E_{\rm beam}$.

Events are permitted to contain a pair of *unmatched* energy clusters in the calorimeter (i.e., those not matched with a charged-particle projection) in the one-prong hemisphere with energy greater than 100 MeV which are consistent with π^0 decay. After π^0 reconstruction, we reject events which have remaining unmatched showers with energy greater than 350 MeV. We further reject events with showers of energy above 100 MeV, provided such showers are well isolated from the nearest track projection (by at least $\sim$30 cm) and have photon-like lateral profiles. These vetoes suppress backgrounds from $q\overline{q}$ events and τ feed across (i.e., τ decay modes containing unreconstructed π^0's or K_L^0's).

The K_S^0 is identified by requiring two of the tracks in the three-prong hemisphere to be consistent with the decay $K_S^0 \to \pi^+\pi^-$. We determine the K_S^0 decay point in the x-y plane by the intersection of the projections of the two tracks onto this plane. This point must lie at least 5 mm from the mean e^+e^- interaction point (IP). We require that the distance between the two tracks in z at the decay point be less than 12 mm to ensure that the tracks form a good vertex in three dimensions. The distance of closest approach to the IP of the line defined by the x-y projection of the K_S^0 momentum vector must be less than 2 mm. The invariant mass of the two tracks, assumed to be pions, must be within 20 MeV of the known K_S^0 mass. For purposes of background subtraction, we define K_S^0 sideband regions which are 30–50 MeV above and below the K_S^0 mass. The data and Monte Carlo (MC) mass distributions are shown in Fig. 1. We find 1482

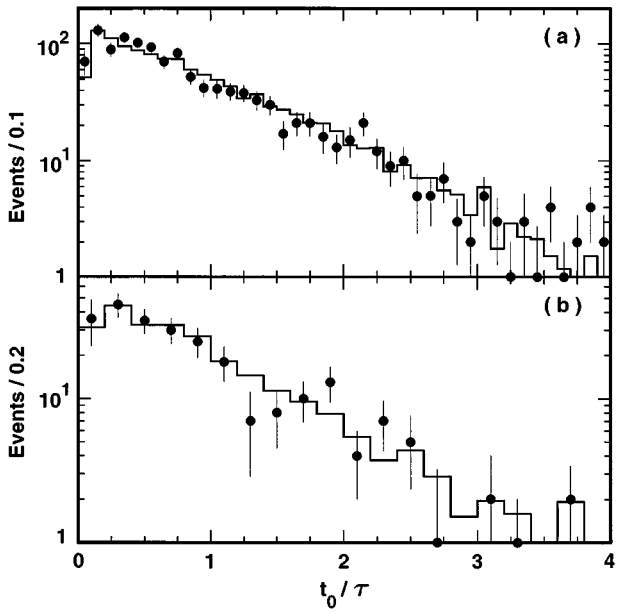

FIG. 3. Normalized proper time distribution (see text) for reconstructed K_S^0 mesons in (a) $\tau^- \to K_S^0 h^- \nu_\tau$ and (b) $\tau^- \to K_S^0 h^- \pi^0 \nu_\tau$ candidate events from data (points) and Monte Carlo (histogram) samples. The corresponding distributions from the K_S^0 mass sideband regions have been subtracted.

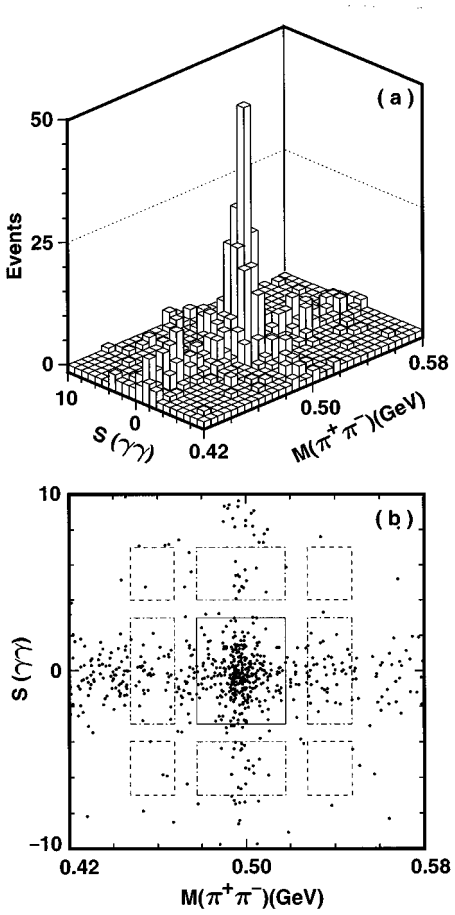

FIG. 4. (a) Lego plot of the distribution in $M_{\pi^+\pi^-}$ vs $S_{\gamma\gamma}$ (see text), for candidate $\tau^- \to K_S^0 h^- \pi^0 \nu_\tau$ decays. (b) Scatter plot of the quantities shown in (a), with signal, sideband, and corner band regions indicated.

events in the signal region and 240 events in the sideband regions. A single event display for one event containing a $K_S^0 \to \pi^+\pi^-$ decay is shown in Fig. 2. In Fig. 3(a), we show the sideband-subtracted distribution of proper time ($d/\gamma v$, where d, v, and γ are the flight distance, velocity, and boost factor of the candidate K_S^0) divided by the known K_S^0 lifetime for events in the $\tau^- \to K_S^0 h^- \nu_\tau$ sample. The distribution deviates only slightly from an exponential, and agrees well with the Monte Carlo prediction.

The selection of $\tau^- \to K_S^0 h^- \pi^0 \nu_\tau$ events proceeds as that for $\tau^- \to K_S^0 h^- \nu_\tau$ events except that a π^0 candidate is required. Such candidates are formed from showers in the three-prong hemisphere with energy greater than 60 MeV and $|\cos\theta| < 0.71$. The mass of the two photons is required to satisfy $|S_{\gamma\gamma}| < 3$, where $S_{\gamma\gamma} = (M_{\gamma\gamma} - M_{\pi^0})/\sigma_{\gamma\gamma}$, and the mass resolution $\sigma_{\gamma\gamma}$ is computed from the photon energy and angular resolution. We define π^0 sidebands to be $\pm(4\text{–}7)$ $\sigma_{\gamma\gamma}$ from the nominal π^0 mass. The data are shown in Fig. 4, with signal and K_S^0/π^0 sideband regions indicated. *Corner* band regions, containing events which lie in the sidebands of both $M_{\pi\pi}$ and $S_{\gamma\gamma}$ distributions, are used to account for possible oversubtraction of combinatoric backgrounds. There are 374 (113) {3} events in the signal (sideband) {corner} regions. The proper time distribution for K_S^0 candidates in these events is shown in Fig. 3(b).

C. Selection of events with a charged kaon

The selection of $\tau^- \to K_S^0 K^- (\pi^0) \nu_\tau$ events is similar to that described above. To improve acceptance, we relax kinematical and fiducial volume cuts. The one-prong track must have $p_T > 0.05 E_{\rm beam}$ and $|\cos\theta| < 0.81$. We require the tracks forming the K_S^0 to have $p_T > 0.05 E_{\rm beam}$ and $|\cos\theta| < 0.90$. The missing momentum must point at least 26° from the beam axis ($|\cos\theta| < 0.90$).

We use the dE/dx measurements in the main drift chamber to identify the charged hadron accompanying the K_S^0 as a possible kaon. To ensure a reliable determination, we require the number of samples (hit drift chamber wires associated with the reconstructed track) used in the dE/dx measurement to be $\geqslant 30$. K-π separation is ambiguous in the momentum region between 1 and 2 GeV. Hence, we require the charged kaon candidate to have a momentum of at least 2.0 GeV. The momentum spectra of the charged kaons (see Fig. 5) are harder than those for the pion background modes. Thus, this momentum cut also enriches the kaon fraction. We obtain no significant gain in sensitivity by including events where the kaon momentum is below 1 GeV. Monte Carlo studies indicate that 36–43% of $\tau^- \to K_S^0 K^- \nu_\tau$ events and 25–28% of $\tau^- \to K_S^0 K^- \pi^0 \nu_\tau$ events are expected to pass the >2.0 GeV cut, where the values reflect the range of predictions from different models.

We determine the number of signal events statistically, by fitting for the number of charged kaons in the $\tau^- \to K_S^0 h^- (\pi^0) \nu_\tau$ sample after application of the cuts de-

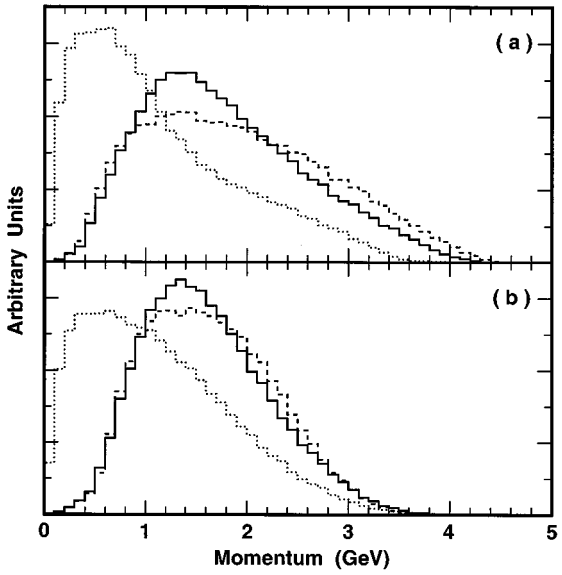

FIG. 5. The momentum spectra of charged kaons from (a) $\tau^- \to K_S^0 K^- \nu_\tau$ and (b) $\tau^- \to K_S^0 K^- \pi^0 \nu_\tau$ events from the generator level Monte Carlo simulation for several models. In (a), ρ-meson dominance in the spectral function is represented by the solid histogram, and the dashed histogram represents a nonresonant model. The momentum spectrum of pions from $\tau^- \to K_S^0 \pi^- \nu_\tau$ is shown as the dotted histogram. In (b), the solid histogram gives the spectrum corresponding to axial-vector $\overline{K}K\pi$ production [via the $a_1(1260)$], while the dashed histogram gives that due to vector $KK\pi$ production (via the ρ'), and the dotted histogram gives the pion momentum spectrum from $\tau^- \to K_S^0 \pi^- \pi^0 \nu_\tau$.

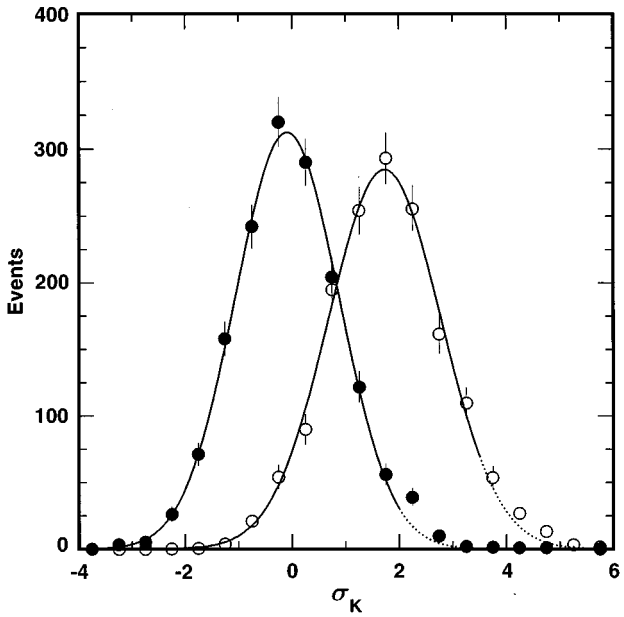

FIG. 6. Distributions in σ_K [see Eq. 5] of high-momentum kaons (filled circles) and pions (open circles) from $D^0 \to K^- \pi^+$ decays, used for calibrating the σ_K distribution. The fits described in the text are indicated by solid curves.

fined above. Specifically, we fit the normalized dE/dx distribution,

$$\sigma_K \equiv \frac{dE/dx_{\rm meas} - dE/dx^K_{\rm exp}(p)}{\sigma_{dE/dx}(p)}, \tag{5}$$

where $dE/dx_{\rm meas}$ and $dE/dx^K_{\rm exp}(p)$ are, respectively, the measured specific ionization and that expected if the charged particle is actually a kaon, and $\sigma_{dE/dx}(p)$ is the expected measurement error. The distribution of σ_K for real K's should be a unit-width Gaussian centered at zero.

To check that this quantity is properly calibrated for real K's and π's, we use a sample of $D^{*+} \to D^0 \pi^+$ decays from the data in which the D^0 decays to $K^- \pi^+$. We select K or π candidates with the same criteria as the hadrons in the $\tau^- \to K_S^0 K^- (\pi^0) \nu_\tau$ sample, including the 2 GeV momentum cut. Above 2 GeV, the dE/dx separation of pions and kaons is very nearly constant.

The D^0 sideband-subtracted distributions for pions and kaons from ~ 2000 $D^{*+} \to D^0 \pi^+$ data events are shown in Fig. 6. The K and π distributions are fit to Gaussians out to $+2\sigma$ and $+3.5\sigma$, respectively. The means for the K and π peaks, as determined from the calibration sample, are -0.04 ± 0.02 and 1.63 ± 0.02, respectively. The corresponding standard deviations are 0.99 ± 0.01 and 1.03 ± 0.02. For the purposes of fitting the τ data, we fix the means to 0.0 and 1.63 and the standard deviations to 1.0 and 1.03, respectively. Uncertainties in the parameters used to fit the dE/dx distributions are included in the systematic error estimate.

In Fig. 7, we plot the σ_K distribution for the 318 $\tau^- \to K_S^0 h^- \nu_\tau$ candidate events passing the cuts described above, including the >2 GeV momentum cut. The fit to pion and kaon response functions yields 111 ± 14 K's and 205

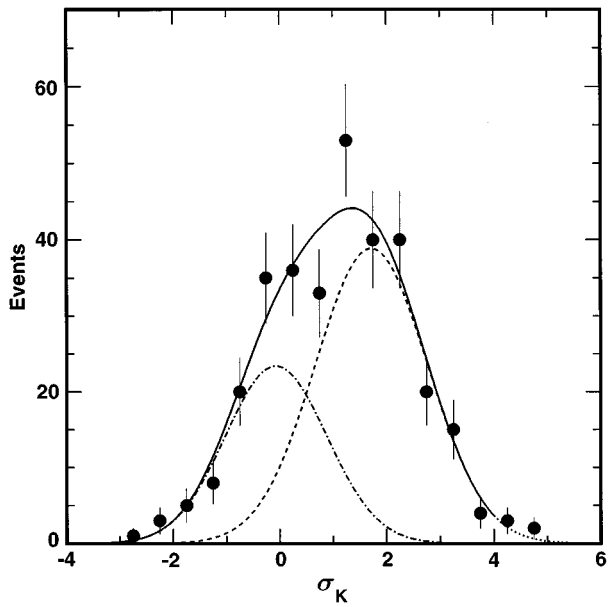

FIG. 7. The σ_K distribution for candidate $\tau^- \to K_S^0 K^- \nu_\tau$ events. The data are shown as points with error bars. The dot-dashed and dashed curves indicate the best fit for the kaon and pion components, respectively, and the solid curve indicates their sum. Points are not shown for bins containing zero entries.

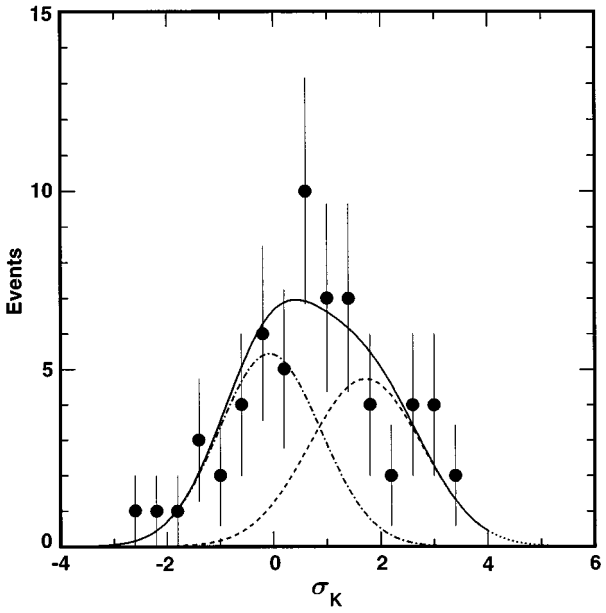

FIG. 8. The σ_K distribution for candidate $\tau^- \to K_S^0 K^- \pi^0 \nu_\tau$ events. The data are shown as points with error bars and the curves are the same as for the previous figure. Points are not shown for bins containing zero entries.

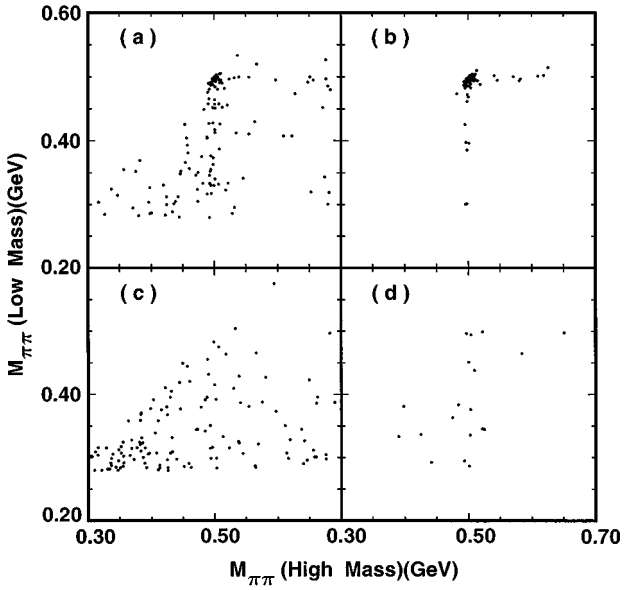

FIG. 9. The invariant mass of the two $K_S^0 \to \pi^+ \pi^-$ candidates (low mass vs high mass) is histogrammed for (a) data, (b) $\tau \to K_S^0 K_S^0 \pi^- \nu_\tau$ signal MC events ($\sim 6\times$ the data yield), (c) τ feed-across background MC ($\sim 3\times$ the data luminosity), and (d) $q\bar{q}$ MC (equivalent luminosity comparable to the data).

± 17 π's. The latter is in good agreement with the number expected from measurements of the $\tau \to K\pi\nu_\tau$ branching fraction (including the one presented here). The fit to the number of K's in the K_S^0 sideband sample gives 0.0 ± 3.0 events.

In the $\tau^- \to K_S^0 h^- \pi^0 \nu_\tau$ sample, the analogous fit to the 63 events yields 32.3 ± 7.1 K's and 31.1 ± 7.1 π's (see Fig. 8). Fits to the numbers of K's in the K_S^0/π^0 sideband and corner band regions give 2 ± 2 and 2 ± 1 events, respectively.

D. Selection of events containing two K_S^0's

For the selection of $\tau^- \to K_S^0 K_S^0 h^- \nu_\tau$ events we require a 1–5 topology with two K_S^0 candidates satisfying criteria similar to those given above. Kinematical and fiducial volume cuts are relaxed as for those in the charged kaon analysis, in order to keep the yield as large as possible. We further allow the x-y flight distance of the K_S^0 candidates to be as small as 3 mm. The selection results in a sample of 52 events in the signal region, 11 events in the sideband region, and 1 event in the corner band region. In Fig. 9, we show two-dimensional plots of the invariant mass of the two $K_S^0 \to \pi^+ \pi^-$ candidates for both data and MC events.

III. MONTE CARLO MODELING

We generate MC samples using a GEANT-based [28] simulation of the CLEO II detector. Effects of accidental activity in the detector are simulated by embedding data collected with a random trigger into MC events. We have produced a sample of about 8×10^6 τ-pair MC events, as well as other samples for specific signal and background decay modes. We also have generated large samples of $q\bar{q}$ [29] and $B\bar{B}$ MC to aid in evaluating these backgrounds.

We use the KORALB/TAUOLA package [30] for $e^+e^- \to \tau^+\tau^-$ production and τ decay with several modifications. Since the situation is complex and the dynamics of the simulation are important, we will describe specifics of the generator in detail.

A. Modeling of decays to two-meson final states

The modeling of the two-meson final states is fairly simple. The hadronic form factor for $\tau^- \to \bar{K}^0 \pi^- \nu_\tau$ decay is modeled as a single P-wave Breit-Wigner resonance, corresponding to $K^*(892)$ dominance (but no $K^{*\prime}$ contribution). We use this parametrization without modification. We added the $\tau^- \to K^0 K^- \nu_\tau$ decay mode since it was not included in Version 2.2 of TAUOLA. We assume the $K^0 K^-$ system to be in a $J^P = 1^-$ state, with a polarization specified according to the $V-A$ structure of weak decays. We investigate both a phase-space spectral function model and one in which the $K^0 K^-$ final state arises from the high-mass tail of the ρ (see Fig. 5).

B. Modeling of decays to three-meson final states

The $\tau^- \to \bar{K}^0 \pi^- \pi^0 \nu_\tau$ decay is presumed to proceed through the axial-vector current via the $K_1(1270)$ and $K_1(1400)$ resonances. We also consider the possibility of a flat spectral function. Although the vector current contribution [perhaps dominated by the $K^*(1410)$] could be substantial, it is essentially neglected in TAUOLA; correspondingly, we do not consider this component in our measurements. However, possible biases due to the model dependence of the detection efficiency are considered in the evaluation of systematic uncertainties (see Sec. V).

Treatment of the $KK\pi$ decays in TAUOLA follows the model of Decker *et al.* [19]. The $\tau \to K\bar{K}\pi\nu_\tau$ decay is imple-

TABLE I. Summary of analysis by decay mode. For each mode we give the total number of events $N_{\rm sig}$, found after K_S^0-sideband and π^0-sideband subtractions, the expected numbers of background events due to non-τ processes $N_{q\bar{q}}$, and τ feed across N_τ, and the detection efficiency, $\mathcal{E}$. Errors are statistical only.

Decay mode	$N_{\rm sig}$	$N_{q\bar{q}}$	N_τ	$\mathcal{E}$ (%)
$\tau^-\to K_S^0 h^-\nu_\tau$	1242 ± 41	38.1 ± 7.1	223 ± 12	6.18 ± 0.05
$\tau^-\to K_S^0 h^-\pi^0\nu_\tau$	264 ± 22	9.5 ± 4.3	5.2 ± 6.8	2.39 ± 0.04
$\tau^-\to K_S^0 K^-\nu_\tau$	111 ± 14	3.6 ± 1.6	7.7 ± 2.8	3.58 ± 0.13
$\tau^-\to K_S^0 K^-\pi^0\nu_\tau$	32.3 ± 7.9	0.8 ± 1.3	0	1.17 ± 0.04
$\tau^-\to K_S^0 K_S^0 h^-\nu_\tau$	42.0 ± 8.0	1.4 ± 2.4	0.0 ± 0.2	5.63 ± 0.19

mented through contributions from both the vector and axial-vector currents [19] with the former dominated by the ρ' and the latter dominated by the $a_1(1260)$. The relevant intermediate states are K^*K and $\rho\pi$ (where again the ρ decays to KK). For the ρ', decay to $KK\pi$ through $\rho\pi$ is forbidden by G-parity conservation. For the a_1 decay, the $\rho\pi$ ($\rho\to KK$) channel is heavily phase-space suppressed. Therefore, in the default parametrization of the $\tau^-\to K^0\bar{K}^0\pi^-\nu_\tau$ decay, $\sim$90% of the decays proceed through K^*K, of which $\sim$30% are from the vector current contribution. For the decay $\tau^-\to K^0K^-\pi^0\nu_\tau$, however, Decker *et al.* [19] suggest that a cancellation between the two possible K^* charge states causes the K^*K contribution to be zero. Since this cancellation is valid only in the chiral limit [10], we have modified TAUOLA to include this decay.

Finally, the decay $\tau^-\to K^0\bar{K}^0K^-\nu_\tau$ could also appear in the $K_S^0K_S^0h^-$ final state. However, we expect this contribution to be negligible due to the Cabibbo and phase-space suppression factors. Consequently, we have not considered this decay in the Monte Carlo generation.

IV. DETERMINATION OF BRANCHING FRACTIONS

For all analyses we determine the branching fraction according to

$$\mathcal{B}(\tau^-\to K_S^0X)=\frac{N_{\rm sig}-N_{q\bar{q}}-N_\tau}{2\,\mathcal{B}(K_S^0\to\pi^+\pi^-)\mathcal{E}\int\sigma_{\tau\tau}\mathcal{L}dt},\qquad(6)$$

where $N_{\rm sig}$ is the number of signal events after sideband subtraction, $N_{q\bar{q}}$ is the expected number of non-τ (predominantly $q\bar{q}$) background events, N_τ is the number of τ feed-across background events, $\sigma_{\tau\tau}$ is the beam-energy-dependent τ-pair production cross section including radiative corrections [30], $\mathcal{L}$ is the luminosity [31], and $\mathcal{E}$ is the efficiency for detecting events where the K_S^0 has decayed to $\pi^+\pi^-$. For the $K_S^0K_S^0h^-$ final state, a second $\mathcal{B}(K_S^0\to\pi^+\pi^-)$ factor appears in the denominator.

The quantities used are summarized in Table I. The efficiency is obtained from Monte Carlo samples generated using the models described in the previous section, combined so that the invariant mass spectra agree with the observed spectra for the given hadronic final states. Backgrounds are estimated using various data and Monte Carlo samples. A significant fraction of the background is accounted for by the sideband subtraction. τ backgrounds comprise the dominant contribution to events populating the sidebands, except in the case of the $K_S^0K_S^0h^-$ channel for which $q\bar{q}$ backgrounds also contribute significantly (see Fig. 9). The contributions $N_{q\bar{q}}$ and N_τ shown in Table I are after sideband subtraction. The residual $q\bar{q}$ background is estimated from the data itself using events where the restrictions on photons in the one-prong hemisphere have been lifted and the invariant mass of the charged track plus the photons in the one-prong hemisphere exceeds the τ mass. Such events are predominantly hadronic, and can be used to estimate the contamination in our selected event sample [32]. For channels with limited statistics, we rely on the $q\bar{q}$ Monte Carlo sample. Backgrounds from $B\bar{B}$ events and two-photon processes are negligible. The amount of τ feed-across background is estimated from the τ Monte Carlo sample. Such backgrounds include contributions to the observed signal from unknown or poorly measured τ decays, such as the contamination of the $K_S^0h^-$ sample by $\tau^-\to K_S^0K_L^0\pi^-\nu_\tau$ decays. We describe the procedures used to bound these backgrounds in the discussion of systematic errors in the following section.

The branching fractions determined in these five analyses are [26]

$$\mathcal{B}(\tau^-\to K^0h^-\nu_\tau)=(0.855\pm0.036\pm0.073)\%,\qquad(7)$$

$$\mathcal{B}(\tau^-\to K^0h^-\pi^0\nu_\tau)=(0.562\pm0.050\pm0.048)\%,\qquad(8)$$

$$\mathcal{B}(\tau^-\to K^0K^-\nu_\tau)=(0.151\pm0.021\pm0.022)\%,\qquad(9)$$

$$\mathcal{B}(\tau^-\to K^0K^-\pi^0\nu_\tau)=(0.145\pm0.036\pm0.020)\%,\qquad(10)$$

$$\mathcal{B}(\tau^-\to K_S^0K_S^0h^-\nu_\tau)=(0.023\pm0.005\pm0.003)\%,\qquad(11)$$

where the first error is due to the statistics of the data samples and the second is the overall systematic uncertainty discussed in detail in Sec. V [33]. For the results (7) to (10), we have multiplied the $\tau^-\to K_S^0X$ branching fractions obtained using Eq. (6) by a factor of 2 to obtain the $\tau^-\to K^0X$ results shown. Since the $K_S^0K_S^0$ fraction in $K^0\bar{K}^0h^-$ events is unknown, the result in (11) is presented as is.

We can determine the branching fractions for the modes $\tau\to K\pi(\pi^0)\nu_\tau$ by taking differences (7)$-$(9) and (8)$-$(10). Taking into account correlated statistical and systematic errors, we obtain

$$\mathcal{B}(\tau^-\to\bar{K}^0\pi^-\nu_\tau)=(0.704\pm0.041\pm0.072)\%,\qquad(12)$$

$$\mathcal{B}(\tau^-\to\bar{K}^0\pi^-\pi^0\nu_\tau)=(0.417\pm0.058\pm0.044)\%.\qquad(13)$$

TABLE II. Summary of systematic uncertainties in percent.

Source	$K_S^0 h^-$	$K_S^0 h^- \pi^0$	$K_S^0 K^-$	$K_S^0 K^- \pi^0$	$K_S^0 K_S^0 \pi^-$
Trigger eff.	0.4	0.2	1	1	1
Track-finding eff.	1.8	1.8	2	2	9
K_S^0-finding eff.	3.0	3.0	3	3	6
Photon veto eff.	2.0	2.0	2	2	2
Detector acceptance	2.1	6.2	2	2	2
Model dependence	0.8	0.6	10	10	2
Non-τ backgrounds	0.7	1.8	4	4	6
τ backgrounds	4.7	0.7	3	0	5
Tag decomposition	5.1	0	0	0	0
π^0 reconstruction	—	3.0	—	3	—
dE/dx uncertainties	—	—	7	7	—
Luminosity	1.0	1.0	1	1	1
τ cross section	1.0	1.0	1	1	1
MC statistics	0.8	1.5	4	3	3
Total	8.5	8.5	15	14	14

Isospin relates the branching fraction for the $\overline{K^0}\pi^-$ final state to that for $K^-\pi^0$. Making use of the 2:1 isospin relation, we compute the weighted average of 3/2 times Eq. (12) above and 3 times the CLEO measurement $\mathcal{B}(\tau^- \to K^- \pi^0 \nu_\tau) = (0.51 \pm 0.10 \pm 0.07)\%$ [24] to infer

$$\mathcal{B}(\tau^- \to (\overline{K\pi})^- \nu_\tau) = (1.11 \pm 0.12)\%. \tag{14}$$

The dominant uncertainties on the measurements entering this average are uncorrelated. To the extent that the $\overline{K\pi}$ system is dominated by the $K^*(892)$ resonance, Eq. (14) gives the $\tau^- \to K^{*-} \nu_\tau$ branching fraction.

V. SYSTEMATIC ERRORS

The systematic errors for the five measurements are summarized in Table II. The total systematic error is determined by summing individual uncertainties in quadrature. Below, we discuss the most significant sources of error individually, focusing primarily on their effects on the systematics-dominated $\tau^- \to K_S^0 h^- \nu_\tau$ branching fraction.

A. Tracking efficiency and $K_S^0 \to \pi^+\pi^-$ finding

We first consider uncertainties arising from imperfect understanding of the performance of the tracking devices and subsequent algorithms applied to reconstruct candidate events. This uncertainty has two components: first, in the efficiency with which each charged-particle trajectory is reconstructed (track finding); and second, in the ability to adequately measure the parameters of the pions forming the K_S^0 candidate (K_S^0 finding). A study of 1–3 topology τ events selected with requirements on only three of the four possible tracks has demonstrated that the detector simulation underestimates the single track-finding efficiency by $\sim 0.4\%$ [34]. We apply a $+0.4\%$ per-track correction to the efficiency, and assign the overall change as the systematic uncertainty, since the origin of this discrepancy is unknown. Because of the higher density of tracks in the $\tau^- \to K_S^0 K_S^0 h^- \nu_\tau$ decay, we assign a more conservative error of 2% per track for the pions from the K_S^0 decays.

The probability that the momenta of the pions from K_S^0 decay have been sufficiently well measured is studied in several ways. First, distributions of quantities used in the selection of K_S^0 candidates show good agreement between data and MC simulation. Furthermore, we have also performed the $K_S^0 h^-$ analysis without applying any of the K_S^0 selection cuts, but plotting the invariant mass of all pairs of oppositely charged pions evaluated at their intersection point. Although the combinatorial background from $\tau^- \to h^- h^+ h^- \nu_\tau$ is quite large in this case, a K_S^0 peak is still evident. We find that the detector simulation reproduces the relative K_S^0 yield to within $\sim 2\%$. Second, we have studied the extent to which tails of the K_S^0 mass resolution are understood by varying the width and position of the signal and sideband regions in the $\pi^+\pi^-$ mass spectrum for the $K_S^0 h^-$ final state. This causes the branching fraction to change by up to $\sim 2\%$. Fitting to the mass spectrum also yields a similar variation, depending on the form of the fit function used. Independent studies of tails in K_S^0 and D^{*+} decays in $q\overline{q}$ events in the data support this result.

Finally, we use the τ MC sample to estimate the extent to which the K_S^0 sideband subtraction fails to properly account for combinatorial background which is assumed to vary smoothly in the K_S^0 signal region. Combining the statistical error in this estimate with the two 2% effects mentioned above leads to an overall error of 3% associated with K_S^0 reconstruction.

B. Photon veto efficiency

Application of the photon veto is effective for rejecting backgrounds, but it also results in some loss of detection efficiency for our signal modes. This is mainly due to interactions of the charged hadrons in the calorimeter, where fragments of hadronic showers can mimic the electromagnetic showers of photons. Additional contributions come from radiative photons and from activity in the calorimeter that is not associated with the primary e^+e^- interaction. All three of these sources are included in the Monte Carlo simu-

lation. We quantify the uncertainty in the simulation of these effects by varying the energy thresholds for the veto (over the range of 80–500 MeV for the photon-like shower veto). Typical variations in $\mathcal{B}(\tau^-\to K^0_S h^-\nu_\tau)$ are $\sim 2\%$, and we assign this as the systematic error.

C. Acceptance and model dependence

We rely on the Monte Carlo simulation for our estimation of the detector acceptance due to geometric and kinematic cuts. This is studied by varying these cuts. We find good agreement between data and Monte Carlo simulation for many distributions of kinematic quantities for most of the modes and assign a 2.1% error associated with detector acceptance. For the $\tau^-\to K^0_S h^-\pi^0\nu_\tau$ channel, however, we observe a systematic shift in the branching fraction as the cut on the minimum track transverse momentum is varied. Such a dependence could be due to inaccuracies in the modeling of the decay (see below), or in the simulation of the detector acceptance. Consequently, for this mode we assign an uncertainty of 6.2%.

The dynamics of the decays being studied also affect the acceptance. For example, in all modes, the simulation reveals that the overall efficiency has some dependence on the invariant mass of the hadronic system. The model-dependence uncertainty is based on the spread in efficiencies predicted with the models described in Sec. III. We also compute the branching fractions by performing efficiency corrections bin-by-bin in the invariant mass distributions. In all cases, the results agree well with those obtained using the nominal models. For the K^-K^0 and $K^-K^0\pi^0$ channels, the model dependence is especially severe, since we rely entirely on the Monte Carlo simulation to estimate the acceptance loss incurred by requiring the K^- momentum to be above 2 GeV.

D. Backgrounds

As shown in Table I, non-τ backgrounds are small. The uncertainties listed in Table II are derived by varying the procedures used to estimate the non-τ backgrounds. For the $K^0_S h^-$ analysis especially, a more significant source of uncertainty is in the level of feed-across backgrounds from other τ decays. We discuss these backgrounds here.

After K^0_S sideband subtraction and non-τ background subtraction, the feed-across background to $\tau^-\to K^0_S h^-\nu_\tau$ is estimated from the MC simulation to account for $18.5\pm 1.0\%$ of the events. This background arises from three sources: τ decays to $K^0_S h^-\pi^0\nu_\tau$ (6.8%) which survive the photon veto; decays to $K^0_S K^0_L h^-\nu_\tau$ (11.3%) in which the K^0_L either passes through the calorimeter without interacting, or interacts and deposits energy clusters which survive the photon veto; and decays to final states which do not contain a K^0_S (0.4%). Uncertainties in the last category are absorbed into the K^0_S-finding errors, since these backgrounds are accounted for only to the extent that the K^0_S-sideband subtraction works. The uncertainty in the first background ($K^0_S h^-\pi^0\nu_\tau$) is 0.9%, dominated by the overall error on our branching fraction determination of that mode. The second background is addressed below.

The $K^0_S K^0_L h^-\nu_\tau$ background error contains contributions from uncertainties in the branching fraction and in the efficacy of the photon veto in rejecting events containing K^0_L's. As noted earlier, we cannot infer the $K^0_S K^0_L h^-\nu_\tau$ branching fraction from our results on $\tau^-\to K^0_S K^0_S h^-\nu_\tau$ without additional theoretical assumptions. We consider a range of possible values of 0.25 to 0.50 for the $K^0_S K^0_S/K^0_S K^0_L$ production fraction R, as constrained by theory [10] and experimental data on substructure in the $K^-K^0\pi^0\nu_\tau$ (see Sec. VI) and $K^-K^+\pi^-\nu_\tau$ [25,35] modes. In addition to our measurement of $\mathcal{B}(\tau^-\to K^0_S K^0_S h^-\nu_\tau)$, there exist results (see Table III) from the L3 Collaboration [36] on $\mathcal{B}(\tau^-\to K^0\overline{K^0}h^-\nu_\tau)$ with small model dependence, and from the ALEPH Collaboration [37] on $\mathcal{B}(\tau^-\to K^0_S K^0_L h^-\nu_\tau)$. Using these three measurements and the range of R above, we assume $\mathcal{B}(\tau^-\to K^0_S K^0_L h^-\nu_\tau)=(0.083\pm 0.027)\%$. The efficiency for accepting this decay is $71\pm 4\%$ that of detecting the signal modes as determined by the Monte Carlo simulation. To this we assign a relative uncertainty of 10% to account for possible inaccurate modeling of K^0_L interactions in the detector. Together these errors result in an uncertainty of 4.5% in the $\tau^-\to K^0 h^-\nu_\tau$ branching fraction, dominated by the uncertainty in $\mathcal{B}(\tau^-\to K^0_S K^0_L h^-\nu_\tau)$.

The uncertainty in the estimate of τ feed-across background to the $K^0_S h^-\pi^0\nu_\tau$ final state consists of two components. First, we consider backgrounds from the known decays $\tau^-\to K^0_S h^-\nu_\tau$ and $\tau^-\to K^0_S K^0_S\pi^-\nu_\tau$. The first mode can contribute if the sideband subtraction fails to properly account for fake π^0's (e.g., if the distribution in $S_{\gamma\gamma}$ is not linear). The second can contribute if one of the K^0_S's decays to $\pi^0\pi^0$ and one of the π^0 decays is reconstructed. Based on uncertainties in the branching fractions for these two decays and on Monte Carlo statistics, we assign a 0.5% uncertainty. Second, we have looked for the decay $\tau^-\to K^0_S h^-\pi^0\pi^0\nu_\tau$ by requiring that two π^0 candidates be found. We find no evidence for such decays beyond the contribution expected from the $\tau^-\to K^0_S K^0_S\pi^-\nu_\tau$ channel noted above. We assign an additional 0.5% uncertainty to cover possible contributions.

E. Tag decomposition

As a consistency check, we have divided each event sample according to the decay of the tag (the one prong) as classified as either $e\nu\overline{\nu}$, $\mu\nu\overline{\nu}$, $h\nu$, or $h\pi^0\nu$. The isolated track is considered an electron if it has $E/p>0.85$, where E is the energy deposited in the calorimeter, and $\sigma_e>-2.0$, where σ_e is the normalized difference between measured and expected values of dE/dx, analogous to σ_K defined earlier. To be considered a muon the isolated track must penetrate at least three nuclear interaction lengths of material to the muon detection system. Tracks accompanied by a π^0 candidate as described in Sec. II B are classified as $h\pi^0\nu$ tags. Decay candidates not classified as leptons or $h\pi^0\nu$ tags are assigned to the $h\nu$ category. Since muons below ~ 1 GeV do not penetrate to the muon detectors they also contribute to this tag classification. Because of the rough equality of tag branching fraction times identification efficiency, the four subsamples are comparable in size.

Comparing the branching fractions computed for each subsample, we find good agreement in all modes, except for the $K^0_S h^-\nu_\tau$ mode. In this channel, we find that the four

subsamples have a χ^2 of 7.2 for three degrees of freedom; notably, the electron-tagged events give a value which is $(26\pm 11)\%$ larger than that from the remaining events. This level of discrepancy persists when cuts are loosened or tightened, and is observed when the data are divided chronologically or according to beam energy. Modification of the analysis to select the kinematically similar but more copious $\tau^-\to h^-h^+h^-\nu_\tau$ decay shows no dependence on the tag decay.

We have considered two possible sources other than statistical fluctuation which could result in such a disagreement: unaccounted-for non-τ backgrounds in the electron-tagged sample, and overestimation of the detection efficiency for the other samples. The latter is unlikely given the checks mentioned above. Since electron-tagged events have better characteristics for triggering, we have investigated whether this could be part of the discrepancy. Studies indicate, however, that the trigger efficiency is above 99% for all tags and is well modeled by the detector simulation.

The possibility of additional background in the electron-tagged sample has also been tested. Background sources which produce events containing one or more electrons include two-photon processes, Bhabha scattering, and beam-gas interactions. We have looked for discrepancies in distributions which are sensitive to these sources, such as missing transverse momentum, total visible energy, and electron momentum, but have found no evidence of contamination. However, most non-τ backgrounds containing a K^0_S will also contain another kaon to balance strangeness. If this were an undetected K^0_L, it would spoil the typical signatures of these backgrounds, mimicking the missing energy and momentum of the neutrinos produced in real τ events.

The tag dependence of the $\tau^-\to K^0h^-\nu_\tau$ branching fraction could also arise from statistical fluctuation. However, the persistence of this variation leads us to conclude that a systematic origin is likely. Thus, we assign a systematic error based on the method used by the Particle Data Group [5] to assign errors to averages of discrepant data. We determine a relative systematic error of 5.1%, which when added in quadrature with the overall statistical error is equal to the square root of the reduced χ^2. For the other decays, no error is assigned.

F. π^0 reconstruction

The efficiency for reconstructing $\pi^0\to\gamma\gamma$ decays depends on the spatial overlap of shower fragments from hadronic interactions in the calorimeter with photon showers. Consequently, knowledge of this efficiency is limited by the extent to which the Monte Carlo program accurately simulates hadronic showers. For τ decays to three charged hadrons plus one π^0, we have established this uncertainty to be 3.0% [34].

G. dE/dx uncertainties

For the modes involving charged kaons, there is a systematic uncertainty associated with the calibration of the dE/dx response for pions and kaons described in Sec. II. The dominant issue is the degree to which pions and kaons in the $D^0\to K^-\pi^+$ calibration sample accurately represent those found in τ decay. Relevant to this issue, dE/dx response depends on: (1) track momentum, (2) path length in the drift cells, varying as $1/\sin\theta$ of the track, and (3) number of drift chamber wire hits providing good measurements. The pions and kaons in the D^0 control sample are similarly distributed in momentum (above 2 GeV) and θ to those from τ decay. However, tracks from the D^0 decay products are more isolated due to the large mass of the D^0, resulting in less frequent sharing of hits among tracks. Consideration of this effect leads us to assign a 7% uncertainty to our estimated kaon identification efficiency.

VI. MASS SPECTRA

The spectral functions for these decays and the resonant substructure are of considerable interest. Here, we present the invariant mass spectra of the various final states studied, and discuss qualitative features of these spectra. In the figures below, the corresponding distributions taken from the K^0_S and π^0 sidebands (where appropriate) have been subtracted to correct for combinatoric backgrounds. Unless otherwise indicated, the spectra have not been corrected for contamination from other backgrounds, for resolution effects, or for distortions due to the mass dependence of the detection efficiency.

A. The $\overline{K}\pi$ system in $\tau^-\to K^0_S h^-\nu_\tau$

The invariant mass distribution for the K^0h^- data sample is shown in Fig. 10, using the pion mass for the h^-. Also shown is the MC prediction with contributions from $K^0_S\pi^-$ and $K^0_S\overline{K}^-$ modes, in addition to the estimated τ feed across and $q\overline{q}$ backgrounds (indicated as a hatched histogram). Both the shape and the normalization of the $K^0_SK^-$ contribution are fixed using our results on this mode (see below). The

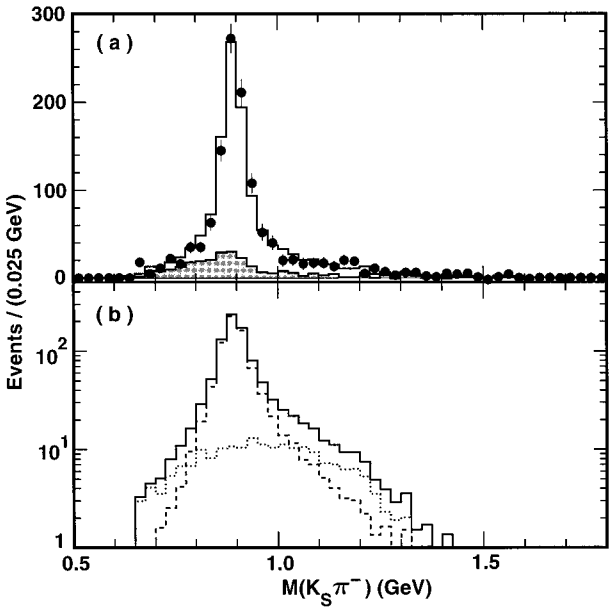

FIG. 10. (a) The $K^0_S\pi^-$ invariant mass distribution for $\tau^-\to K^0_Sh^-\nu_\tau$ decays in the data (points) and MC simulation, where the total background fraction as predicted from the MC sample is shown as hatched. (b) Contributions to the total (solid) signal MC sample from $K^0_S\pi^-$ (dashed) and $K^0_SK^-$ (dotted) final states.

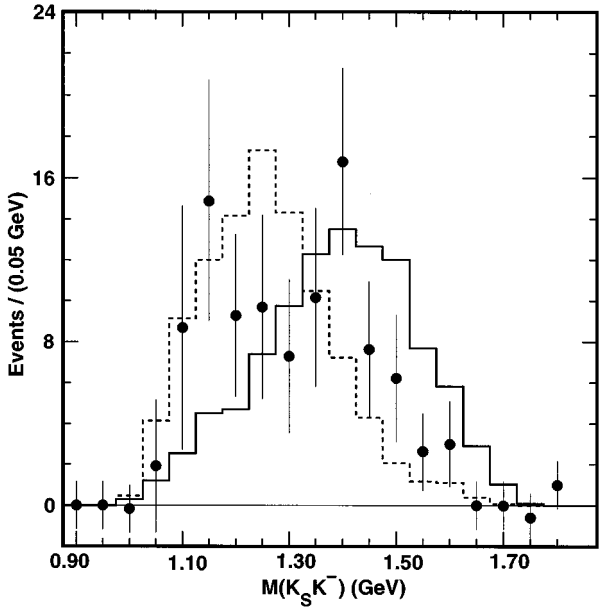

FIG. 11. The invariant mass distribution for $\tau^- \to K^0 K^- \nu_\tau$ events is shown for data (points) the MC sample for a flat spectral function (solid histogram), and the MC sample with a $\rho \to K\overline{K}$ model (dashed histogram). Each MC model is normalized to the number of events in the data.

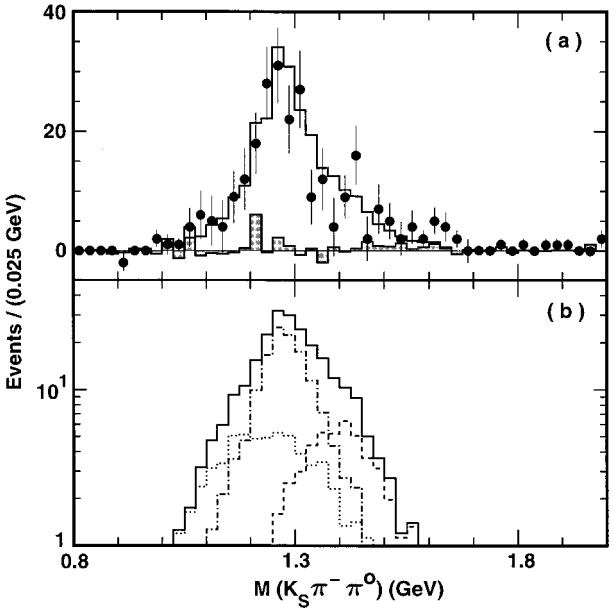

FIG. 12. (a) The $K^0_S \pi^- \pi^0$ invariant mass distribution for $\tau^- \to K^0_S h^- \pi^0 \nu_\tau$ decays in the data (points) and MC simulation, where the total background fraction as predicted from the MC sample is shown as hatched. (b) Contributions to the total (solid) signal MC sample from $K_1(1270)$ (dot-dashed), $K_1(1400)$ (dashed), and $K^- K^0_S \pi^0$ (dotted) final states.

data are dominated by the $K^*(892)$ resonance, though further analysis is required to quantify additional resonant ($K^{*\prime}$) and nonresonant contributions.

B. The $\overline{K}K$ system in $\tau^- \to K^- K^0_S \nu_\tau$

Since there are two pseudoscalars in the final state, the decay $\tau^- \to K^0 K^- \nu_\tau$ should proceed through the vector current, though there are different expectations concerning the spectral function. In Fig. 11, we show the data with the MC prediction for a flat spectral function and a $\rho \to K\overline{K}$ model superimposed. The entries in this figure are derived from separate fits to the σ_K distribution for events in each mass bin. The data prefer the resonant model; however, neither model provides a satisfactory description of the data.

C. The $\overline{K}\pi\pi$ system in $\tau^- \to K^0_S h^- \pi^0 \nu_\tau$

The situation for the $K^0_S h^- \pi^0$ final state is quite complicated. As discussed previously, this state should have major contributions from $K_1(1270)$, $K_1(1400)$, and $K^0_S K^- \pi^0$. We show the invariant mass distribution for $K^0_S h^- \pi^0$ events in Fig. 12, again assuming the pion mass for the charged hadron accompanying the K^0_S. Overlaid is the MC prediction containing contributions from the three channels, as well as the various backgrounds (indicated by the hatched histogram). The data are consistent with a K_1 intermediate state with the $K_1(1270)$ contributing substantially more than that from the $K_1(1400)$, contrary to (but not inconsistent with) results presented by the TPC/2γ Collaboration [38]. The possible vector contribution from $K^*(1410)$ precludes quantitative conclusions about the amount of $K_1(1400)$ without more detailed study.

D. The $\overline{K}K\pi$ system in $\tau^- \to K^0_S K^- \pi^0 \nu_\tau / K^0_S K^0_S h^- \nu_\tau$

We study the structure in the $K\overline{K}\pi$ final state using both the $K^0_S K^- \pi^0$ and $K^0_S K^0_S h^-$ final states. In Fig. 13, we show the invariant mass of the $K^0 K^- \pi^0$ system for the data. As in Fig. 11, the entries are derived from fits to the σ_K distribu-

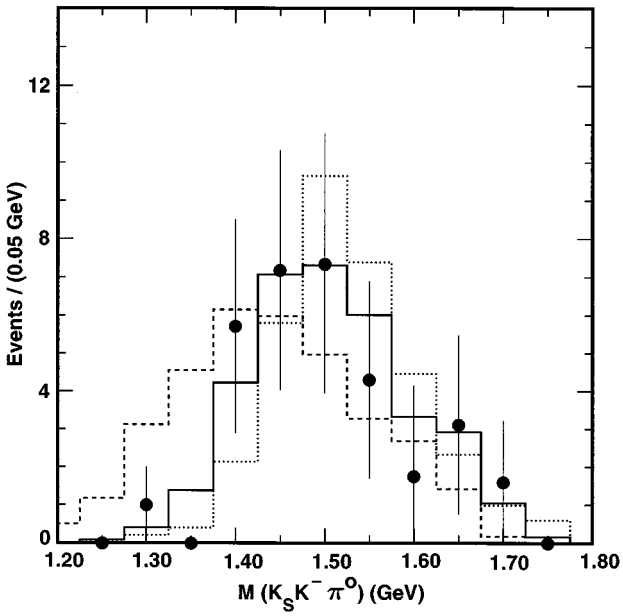

FIG. 13. The invariant mass distribution for $\tau^- \to K^0 K^- \pi^0 \nu_\tau$ events is shown for data (points), axial-vector (a_1) MC sample, and vector (ρ') MC sample. The $a_1 \to K^* K$ and $\rho' \to K^* K$ models are shown as the solid and dotted histograms, respectively. The $a_1 \to \rho\pi$ model is shown as the dashed histogram.

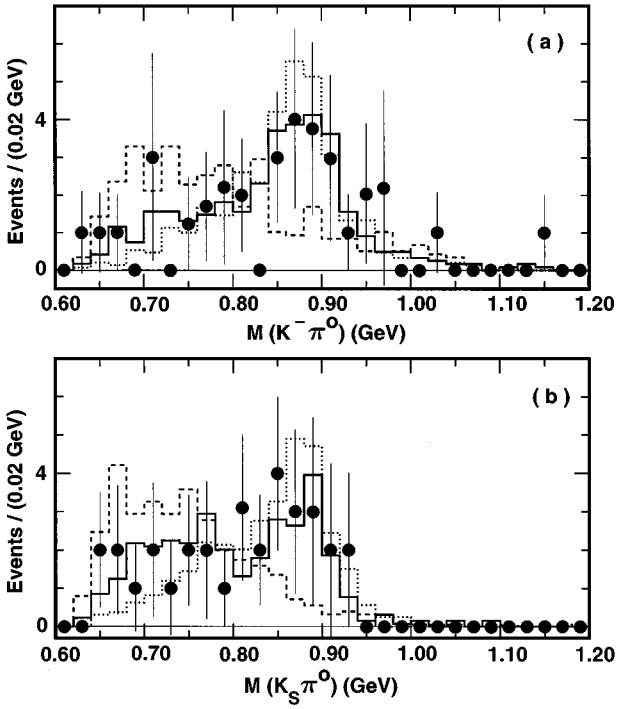

FIG. 14. The (a) $K^-\pi^0$ and (b) $K^0_S\pi^0$ invariant mass distributions for $\tau^-\to K^0K^-\pi^0\nu_\tau$ events for data (points) and MC simulation. The histograms are the same as for the previous figure.

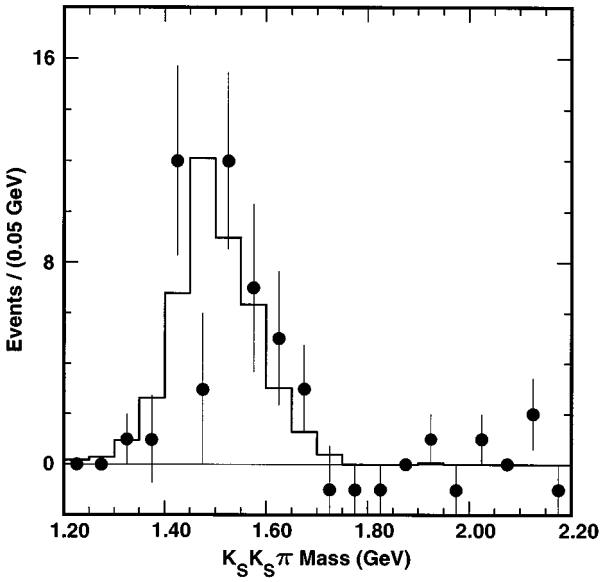

FIG. 15. The $K^0_SK^0_S\pi^-$ invariant mass distribution for $\tau^-\to K^0_SK^0_Sh^-\nu_\tau$ events is shown for data (points) and the MC prediction (histogram).

tions for events in each mass bin. This and the following plots are K^0_S/π^0 sideband subtracted and corrected for τ feed-across background but not $q\overline{q}$ background due to limited Monte Carlo statistics. Also shown are the MC expectations for vector production of K^*K and axial-vector production of K^*K and $\rho\pi$ intermediate states. The data suggest that the K^*K contribution is significant. This is contrary to the expectations from the chiral model of Ref. [19], and more consistent with the model of Ref. [10] which considers both K^*K and $\rho\pi$ intermediate states. This is further supported by the fact that the branching fraction [Eq. (10)] is comparable to other $K\overline{K}\pi$ charge states [39], as expected from K^*K dominance. The limited statistics preclude discrimination between vector and axial-vector production of K^*K, however.

In order to investigate the direct evidence for a K^*K intermediate state, we show the $K\pi^0$ invariant masses in Fig. 14. Again, the data are consistent with K^*K dominance. On the basis of these plots alone, however, one cannot rule out a significant contribution from $\rho\pi$.

The mass distribution for the $K^0_SK^0_Sh^-$ channel, along with the expectation from the Monte Carlo simulation, is shown in Fig. 15. As in the $K^-K^0\pi^0$ case, there are too few events to distinguish between different models for this decay. The spectrum shown is relatively background free: non-τ backgrounds have been accounted for statistically by the K^0_S sideband subtraction, as is evident by the net number of events above the τ mass. Though more restrictive requirements on the K^0_S reconstruction eliminate these background events altogether, albeit with some loss of efficiency, no event has sufficiently high mass for an interesting constraint on the τ neutrino mass.

In Fig. 16, the $K^0_S\pi^-$ invariant mass is plotted for each of the two combinations possible in each $\tau^-\to K^0_SK^0_Sh^-\nu_\tau$ event. The data are consistent with being entirely due to K^*K, the entries outside of the K^* mass region representing the *wrong* $K^0_S\pi^-$ combination. The distribution is in good agreement with the spectrum from the Monte Carlo simulation which is dominated by K^*K production of $K^0_SK^0_S\pi^-$.

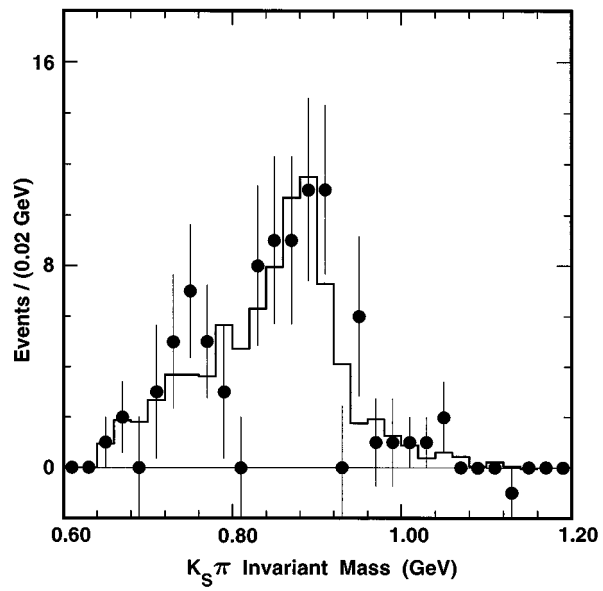

FIG. 16. The $K^0_S\pi^-$ invariant mass distribution for $\tau^-\to K^0_SK^0_Sh^-\nu_\tau$ events (two entries per event) is shown for data (points) and MC simulation (histogram).

TABLE III. Present status of exclusive branching fraction measurements for the various (Kh) and (Khh) modes. Measurements of related semiinclusive decay modes and unpublished results are not listed (see Refs. [5] and [4], respectively). Also shown are relevant theoretical predictions (corresponding to decay mode, not experiment).

τ decay mode	Experiment	$\mathcal{B}$(%)	Theory (%)
$\overline{K^0}\pi^-$	ALEPH 95 [40]	$0.79\pm0.10\pm0.09$	
	L3 95 [36]	$0.95\pm0.15\pm0.06$	
	This analysis	$0.704\pm0.041\pm0.072$	
$K^-\pi^0$	CLEO 94 [24]	$0.51\pm0.10\pm0.07$	
	DELPHI 94 [41]	0.57 ± 0.23	
	ALEPH 95 [40]	$0.52\pm0.04\pm0.05$	
K^0K^-	TPC/2γ 87 [42]	<0.26 95% C.L.	0.11 [10]
	ALEPH 95 [40]	$0.26\pm0.09\pm0.02$	0.12 ± 0.03 [15]
	This analysis	$0.151\pm0.021\pm0.022$	0.16 ± 0.02 [16]
$\overline{K^0}\pi^-\pi^0$	ALEPH 95 [40]	$0.32\pm0.11\pm0.05$	
	This analysis	$0.417\pm0.058\pm0.044$	0.96 [10]
$K^-\pi^+\pi^-$	DELCO 85 [20]	$0.22^{+0.16}_{-0.13}\pm0.05$	
	TPC/2γ 94 [38]	$0.58^{+0.15}_{-0.13}\pm0.12$	0.77 [10]
$K^-\pi^0\pi^0$	CLEO 94 [24]	$0.14\pm0.10\pm0.03$	
	ALEPH 95 [40]	$0.08\pm0.02\pm0.02$	0.14 [10]
$\overline{K^{*0}}\pi^-$	CLEO 90 [25]	$0.38\pm0.11\pm0.13$	
	ARGUS 95 [35]	$0.25\pm0.10\pm0.05$	
$K^0K^-\pi^0$	ALEPH 95 [40]	$0.10\pm0.05\pm0.03$	
	This analysis	$0.145\pm0.036\pm0.020$	0.16 [10]
$K^-K^+\pi^-$	DELCO 85 [20]	$0.22^{+0.17}_{-0.11}\pm0.05$	
	TPC/2γ 94 [38]	$0.15^{+0.09}_{-0.07}\pm0.03$	0.20 [10]
$K^0\overline{K^0}\pi^-$	L3 95 [36]	$0.31\pm0.12\pm0.04$	0.20 [10]
$K^0_SK^0_L\pi^-$	ALEPH 95 [37]	$0.13\pm0.04\pm0.02$	0.10 [10]
$K^0_SK^0_S\pi^-$	This analysis	$0.023\pm0.005\pm0.003$	0.048 [10]
$K^{*0}K^-$	CLEO 90 [25]	$0.32\pm0.08\pm0.12$	
	ARGUS 95 [35]	$0.20\pm0.05\pm0.04$	

This is as expected since the $\rho\pi$ intermediate state is not expected to contribute to this decay.

VII. DISCUSSION

Many of the recent measurements for exclusive $\tau^-\to(KX)^-\nu_\tau$ decay modes are shown in Table III. Within errors and to the extent that comparisons can be made, there is a general agreement between our measurements and other experimental results. Below we discuss our results in the context of the experimental situation and theoretical considerations.

A. Decays containing two mesons

For the $\overline{K\pi}$ final state, isospin symmetry demands that the $\overline{K^0}\pi^-$ and $K^-\pi^0$ decays occur in the ratio 2:1 independent of dynamics. Our value for $\mathcal{B}(\tau^-\to\overline{K^0}\pi^-\nu_\tau)$ is low relative to expectations from the $K^-\pi^0$ measurements, but in good agreement with the other results on $\overline{K^0}\pi^-$.

As mentioned in the Introduction, $\mathcal{B}(\tau^-\to(\overline{K\pi})^-\nu_\tau)$ is expected to be $(1.20\pm0.02)\%$, based on a crude application of the DMO sum rule. Combining the result on $\tau^-\to K^0_S\pi^-\nu_\tau$ presented here with the result from CLEO on $\tau^-\to K^-\pi^0\nu_\tau$ presented previously [24], we have measured it to be $(1.11\pm0.12)\%$. Since the calculation did not include the significant non-ρ contributions to the nonstrange vector spectral function, which would increase the prediction to $\sim2\%$, we conclude that there must also be a significant non-$\overline{K\pi}$ contribution (such as $\overline{K\pi\pi}$) to the $S=1$ vector spectral function, if the sum rule is to hold. Qualitative examination of the $K\pi$ mass spectrum (see Fig. 10) in $\tau^-\to K^0_Sh^-\nu_\tau$ de-

cays shows that contributions from $\tau^- \to K^*(892)^- \nu_\tau$ and $\tau^- \to K^0 K^- \nu_\tau$ dominate this spectrum. A quantitative analysis is needed to establish the K^* parameters and determine whether there is evidence for $K^*(1410)$ production (which would also contribute to the $K\pi\pi$ final state).

We have measured the branching fraction of the nonstrange decay $\tau^- \to K^0 K^- \nu_\tau$ to be $(0.151 \pm 0.021 \pm 0.022)\%$, consistent with the predictions from CVC of $(0.12 \pm 0.03)\%$ [15] and $(0.16 \pm 0.02)\%$ [16]. Neither the nonresonant model nor the ρ-dominant model reproduces the $K^0 K^-$ mass spectrum particularly well; however, more data are needed to make a strong statement on this issue.

B. Decays to three mesons

For the three-meson $\overline{K}\pi\pi$ and $K\overline{K}\pi$ decays, comparison of experimental results is less straightforward. Relations among the various charge states due to isospin depend on the dynamics, and only limited constraints can be derived without making assumptions [17]. Untangling of the dynamics is complicated by the fact that both the vector and axial-vector hadronic current can contribute to these decays.

The production of $\overline{K^0}\pi^-\pi^0$, $K^-\pi^+\pi^-$, and $K^-\pi^0\pi^0$ states would occur in the ratio 4:4:1 (2:1:0) from isospin, if the intermediate state is dominated by $K^*\pi$ ($K\rho$). The nonzero value for $K^-\pi^0\pi^0$ and evidence for $\overline{K^{*0}}\pi^-$ production indicate a large $K^*\pi$ contribution. Since the sum of average branching fractions for the three charge states exceeds 1.5 times the mean of the $\overline{K^{*0}}\pi^-$ branching fraction values, however, the presence of some $K\rho$ production is also likely. Furthermore, if the $K_1(1270)$ is a major source of $K\pi\pi$, as suggested by Fig. 12, one would expect the contribution from $K\rho$ to be significant.

Because there is no clear theoretical prediction for the $\tau \to K\pi\pi\nu_\tau$ branching fraction, our result is difficult to interpret. Our value for $\mathcal{B}(\tau^- \to \overline{K^0}\pi^-\pi^0\nu_\tau)$ of $(0.417 \pm 0.058 \pm 0.044)\%$ is roughly a factor of 2 lower than the predictions from the model of Finkemeier and Mirkes [10]. From the $K\pi\pi$ mass spectrum it appears likely that there is a significant contribution from the axial-vector $K_1(1270)$. However, this contribution does not saturate the high-mass end of the distribution. To know whether the high-mass events are due to production of the axial-vector $K_1(1400)$ or the vector $K^*(1410)$ will require a study of the angular distribution of the $K^*\pi$ system.

Similarly, for the nonstrange decay $\tau \to \overline{K}K\pi\nu_\tau$, comparison and interpretation of branching fractions is difficult. From isospin, we expect that the production ratio for $K^-K^0\pi^0$, $K^-K^+\pi^-$, and $K^0\overline{K^0}\pi^-$ final states would be 2:1:1 (1:1:1) if the substructure were dominated by $\rho\pi$ (K^*K). Taken together, the results listed in Table III and the mass spectra shown in Figs. 13 and 14 suggest that $KK\pi$ production occurs at a significant level through K^*K. The model of Ref. [10] predicts branching fractions for $\tau^- \to K^0 K^- \pi^0 \nu_\tau$ close to our measurement of $(0.145 \pm 0.036 \pm 0.020)\%$, but somewhat higher values for $\tau^- \to K_S^0 K_S^0 \pi^- \nu_\tau$ than what we observe.

VIII. CONCLUSIONS

To summarize, we have reported on analyses of five τ decay modes involving K_S^0 mesons using data obtained with the CLEO II detector. We have measured branching fractions for these modes with better precision than those of previous measurements and have presented invariant mass spectra for comparison with theoretical models. These results shed some light on the the complicated dynamics of τ decays to final states containing kaons. However, more experimental work is needed to resolve the outstanding issues.

ACKNOWLEDGMENTS

We gratefully acknowledge the effort of the CESR staff in providing us with excellent luminosity and running conditions. We also acknowledge useful discussions with Erwin Mirkes and the late Roger Decker. J.P.A, J.R.P., and I.P.J.S. thank the NYI program of the NSF, G.E. thanks the Heisenberg Foundation, K.K.G., M.S., H.N.N., T.S., and H.Y. thank the OJI program of the DOE, J.R.P., K.H., and M.S. thank the A.P. Sloan Foundation, and A.W. and R.W. thank the Alexander von Humboldt Stiftung for support. This work was supported by the U.S. National Science Foundation, the U.S. Department of Energy, and the Natural Sciences and Engineering Research Council of Canada.

[1] T. Das, V. S. Mathur, and S. Okubo, Phys. Rev. Lett. **18**, 761 (1967); **19**, 859 (1967).
[2] Y. S. Tsai, Phys. Rev. D **4**, 2821 (1971).
[3] Throughout this article, charge-conjugate reactions are implied.
[4] B. K. Heltsley, In *Tau 94*, Proceedings of the Third Workshop on Tau Lepton Physics, Montreaux, Switzerland, 1994, edited by L. Rolandi [Nucl. Phys. B (Proc. Suppl.) **40**, 413 (1995)].
[5] Particle Data Group, L. Montanet *et al.*, Phys. Rev. D **50**, 1173 (1994), and 1995 off-year partial update for the 1996 edition (URL: http://pdg.lbl.gov/).
[6] J. H. Kühn and A. Santamaria, Z. Phys. C **48**, 445 (1990).
[7] L. M. Barkov *et al.*, Nucl. Phys. **B256**, 365 (1985).
[8] A. J. Weinstein, in *Tau 94* [4], p. 163.
[9] CLEO Collaboration, ''A Study of the hadronic current in tau decays to vector mesons'' (in preparation).
[10] M. Finkemeier and E. Mirkes, Z. Phys. C **69**, 243 (1996).
[11] R. D. Peccei and J. Solà, Nucl. Phys. **B281**, 1 (1987).
[12] J. F. Donoghue and B. R. Holstein, Phys. Rev. D **46**, 4076 (1992).
[13] S. Weinberg, Phys. Rev. Lett. **18**, 507 (1967).
[14] M. Suzuki, Phys. Rev. D **47**, 1252 (1993); H. J. Lipkin, Phys. Lett. B **303**, 119 (1993); E. H. Berger and H. J. Lipkin, **189**, 226 (1987).
[15] S. I. Eidelman and V. N. Ivanchenko, Phys. Lett. B **257**, 437 (1991); see also S. I. Eidelman and V. N. Ivanchenko, Nucl. Phys. B (Proc. Suppl.) **40**, 131 (1995).
[16] S. Narison and A. Pich, Phys. Lett. B **304**, 359 (1993).

[17] F. J. Gilman and S. H. Rhie, Phys. Rev. D **31**, 1066 (1985).
[18] J. J. Gomez-Cadenas, M. C. Gonzalez-Garcia, and A. Pich, Phys. Rev. D **42**, 3093 (1990).
[19] R. Decker, E. Mirkes, R. Sauer, and Z. Was, Z. Phys. C **58**, 445 (1993).
[20] DELCO Collaboration, G. B. Mills *et al.*, Phys. Rev. Lett. **54**, 624 (1985).
[21] ARGUS Collaboration, H. Albrecht *et al.*, Phys. Lett. B **202**, 149 (1988); **292**, 221 (1992).
[22] CLEO Collaboration, D. Cinabro *et al.*, Phys. Rev. Lett. **70**, 3700 (1993).
[23] ALEPH Collaboration, D. Buskulic *et al.*, Phys. Lett. B **349**, 585 (1995).
[24] CLEO Collaboration, M. Battle *et al.*, Phys. Rev. Lett. **73**, 1079 (1994).
[25] CLEO Collaboration, M. Goldberg *et al.*, Phys. Lett. B **251**, 223 (1990).
[26] In the inclusive measurements involving a neutral kaon plus a charged hadron, the flavor of the kaon depends on the identity of the charged hadron. For ease of notation, we use K^0h^- to denote the sum of contributions from processes containing $\overline{K^0}\pi^-$ and K^0K^- particle combinations.
[27] CLEO Collaboration, Y. Kubota *et al.*, Nucl. Instrum. Methods Phys. Res, Sect A **320**, 66 (1992).
[28] R. Brun *et al.*, GEANT 3.15, Report No. CERN DD/EE/84-1 (unpublished).
[29] JETSET 7.3: T. Sjöstrand and M. Bengtsson, Comput. Phys. Commun. **43**, 367 (1987).
[30] We use KORALB (v.2.2)/ TAUOLA (v.2.4). References for earlier versions are: S. Jadach and Z. Was, *ibid.* **36**, 191 (1985); **64**, 267 (1991); S. Jadach, J. H. Kühn, and Z. Was, *ibid.* **64**, 275 (1991); **70**, 69 (1992); **76**, 361 (1993).
[31] CLEO Collaboration, G. Crawford *et al.*, Nucl. Instrum. Methods Phys. Res., Sect. A **345**, 429 (1994).
[32] CLEO Collaboration, M. Procario *et al.*, Phys. Rev. Lett. **70**, 1207 (1993).
[33] Uncertainties because of the finite statistics of data and Monte Carlo samples used to estimate detection efficiencies and backgrounds are included in the systematic uncertainty.
[34] CLEO Collaboration, R. Balest *et al.*, Phys. Rev. Lett. **75**, 3809 (1995).
[35] ARGUS Collaboration, H. Albrecht *et al.*, Z. Phys. C **68**, 215 (1995).
[36] L3 Collaboration, M. Acciarri *et al.*, Phys. Lett. B **352**, 487 (1995).
[37] ALEPH Collaboration, EPS95 Ref. EPS0448, contribution to the International Europhysics Conference on High Energy Physics, Brussels, 1995 (unpublished).
[38] TPC/2γ Collaboration, D. A. Bauer *et al.*, Phys. Rev. D **50**, R13 (1994).
[39] Heltsley [4] finds a world average $B(\tau^-\to K^+K^-\pi^-\nu_\tau)=(0.20\pm0.07)\%$.
[40] ALEPH Collaboration, D. Buskulic *et al.*, Report No. CERN-PPE/95-140, 1995 (unpublished). See also D. Buskulic *et al.*, Phys. Lett. B **332**, 209 (1994); **332**, 219 (1994).
[41] DELPHI Collaboration, P. Abreu *et al.*, Phys. Lett. B **334**, 435 (1994).
[42] TPC/2γ Collaboration, H. Aihara *et al.*, Phys. Rev. Lett. **59**, 751 (1987).